Sixth International Symposium on Marine Propulsors
smp'19, Rome, Italy, May 2019

Effect of Gap Flow Model on Hydrodynamic Performance of Pump jet Propulsor*

Kaiqiang Weng[1], Chao Wang[1]

[1]College of Shipbuilding Engineering, Harbin Engineering University, Harbin, PR China

ABSTRACT

There is a strong gap flow in the pump jet propulsor, in order to predict the hydrodynamic performance of the pump jet propulsor, the steady-state hydrodynamic disturbance model was established by the panel method. The pump jet propulsor was divided into two systems, rotor-hub and stator-duct, and inter-system interference was considered by induced velocity. Based on the actual situation of the internal flow of the pump jet propulsor, a gap flow model suitable for the flat-topped blade was proposed. Comparing the results of pressure, circular, and thrust performance, it was found that when the influence of gap flow model is considered, the overall circular distribution of rotor blade and tip load are closer to the actual situation, and the performance curve is in good agreement with the viscous flow, which shows that this method can effectively predict the steady hydrodynamic performance of the pump jet propulsor.

Keywords

panel method; pump jet propulsor; performance prediction; gap flow model

1 INTRODUCTION

As a new type of combined propeller, pump-jet propulsor has been widely used in nuclear submarines and torpedoes due to its high propulsion efficiency, low noise and high critical speed. At present, the numerical analysis method based on potential flow theory has been successfully used for hydrodynamic performance prediction with stator ducted propellers, such as the lift surface vortex method (Hughes M J et al 1991) and the panel method (Kawakita C et al 1998) adopted by Hughes et al. and Kawakita, respectively. The gap between the pump jet propulsor rotor and the duct is usually between 1% and 3% of the rotor tip radius. The flow in the small gap region appears as a true viscous flow, and the use of the potential flow assumption causes the rotor tip load to be close to zero, which is not in line with the actual situation. In view of the above gap flow, Mchugh used the vortex lattice method to establish a permeation sheet model to improve the prediction results of the tip load of the duct blade (Mchugh et al 1997). Based on this, Baltazar et al. discussed the influence of the gap flow model on the prediction results of the ducted propeller (Baltazar J et al 2015). Considering the compact layout of the pump jet propulsor, the effect of the gap flow is not only limited to the rotor tip, but even causes the flow field of the entire system to change.

In this paper, the surface panel method based on potential flow theory is used to establish the numerical model of pump-jet propulsor. The gap flow model is added to the original numerical model. The effects of the gap flow model on the calculation results are analyzed from the aspects of pressure distribution, circular distribution and performance index.

2 Numerical model

The theoretical method of establishing the numerical model in this paper was based on velocity potential low-order surface panel method, in which the discrete elements on the surface of the object are hyperbolic elements, and the singularities arranged on the elements are the mixed distribution of source and dipole. The numerical model of the pump jet propulsor was established by solving the basic equations of a lifting body, and the gap flow model was added to the original model. The basic equation is as follows:

$$4\pi E\varphi(P)=\iint_{S_b+S_w+S_\infty}\left[\varphi(Q)\frac{\partial}{\partial n_Q}(\frac{1}{R_{PQ}})-\frac{\partial\varphi(Q)}{\partial n_Q}\frac{1}{R_{PQ}}\right]\mathrm{d}S \qquad (1)$$

where, S is the boundary of the fluid, which is composed of the object surface S_b, the wake vortex surface S_w, and the outer boundary surface. Q is the arbitrary control point on the boundary surface S. R_{PQ} is the straight line distance between two points P and Q. $\partial\varphi(Q)/\partial n_Q$ is the normal derivative of the point velocity potential—satisfying the non-penetrating surface condition. E is the Green formula parameter—the value of E is 0 when the point P is within S, 0.5 when P is on S, and 1 when P is outside S.

2.1 Numerical model of the pump jet propulsor

The components of the pump jet propulsor are divided into two independently existing lift bodies in the same coordinate system, rotor-hub system and stator-duct

system, as shown in Fig.1. The two systems respectively constitute the basic equations, and the interaction between systems takes into account the perturbation of the flow field around each system, while the interference effect is expressed in the form of induced speed. The equations of velocity and induced velocity of each system are solved in turn. By way of induced velocity loop iteration, the numerical solutions of both systems reach the convergence criterion, so as to obtain the overall calculation results of the pump jet propulsor. The following is a description of the velocity potential and the induced velocity for the stator-to-hub system and the stator-to-duct system of the rear stator pump jet propulsor model and the front stator pump jet propulsor model.

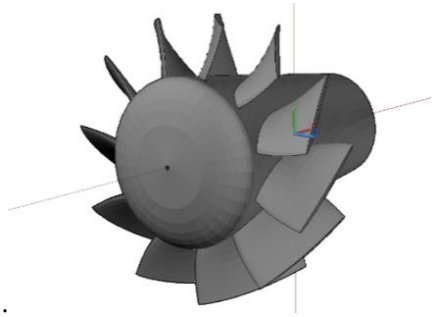

(a) Rotor-Hub System

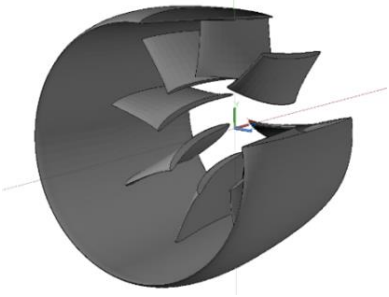

(b) Stator-duct System

Fig.1Rear stator pump schematics. (a) Rotor-hub system. (b) Stator-duct system.

According to Eq.(1), the equations for solving the velocity potential of stator-duct system and rotor-hub system at the boundary are expressed as:

$$2\pi\varphi^k(P)=\iint_{S_s+S_d}\varphi^k(Q)\frac{\partial}{\partial n_Q}(\frac{1}{R_{PQ}})\mathrm{d}S+\iint_{S_{ws}+S_{wd}}\Delta\varphi^k(Q_1)\frac{\partial}{\partial n_{Q_1}}(\frac{1}{R_{PQ_1}})\mathrm{d}S+\iint_{S_s+S_d}\left((\overrightarrow{V_0}+\overrightarrow{V_{sd,rh}^k})\cdot\overrightarrow{n_Q}\right)(\frac{1}{R_{PQ}})\mathrm{d}S \tag{2}$$

$$2\pi\varphi^k(P)=\iint_{S_r+S_h}\varphi^k(Q)\frac{\partial}{\partial n_Q}(\frac{1}{R_{PQ}})\mathrm{d}S+\iint_{S_{wr}}\Delta\varphi^k(Q_1)\frac{\partial}{\partial n_{Q_1}}(\frac{1}{R_{PQ_1}})\mathrm{d}S+\iint_{S_r+S_h}\left((\overrightarrow{V_0}+r\overrightarrow{\Omega_\theta}+\overrightarrow{V_{rh,sd}^k})\cdot n_Q\right)(\frac{1}{R_{PQ}})\mathrm{d}S \tag{3}$$

where S_s, S_d, S_r, and S_h are the stator surface, duct surface, rotor surface, and hub surface, respectively; S_{ws}, S_{wd}, and S_{wr} are the wake vortex surfaces of the corresponding components; P and Q are arbitrary control points on the boundary S; R_{PQ} is the straight line distance between two points P and Q; $\vec{n}$ is the unit normal vector of the object surface, pointing to the flow field; $\Delta\varphi$ is the velocity potential jump across the wake vortex surface; $\vec{\Omega}_\theta$ is the rotational angular velocity of the propeller; k is the kth iteration; $\vec{V}_{sd,rh}$ represents the induced velocity of the rotor-hub system on the surface of the stator and the duct, as part of the stator-duct system relative inflow velocity, and $\vec{V}_{rh,sd}$ is in the opposite direction.

2.2 Gap flow model

Due to the viscous effect of the rotor end face and the boundary layer of the inner wall of the duct, the fluid velocity in the gap region is attenuated, which changes the load distribution of the blade tip and affects the overall circular distribution of the blade. The permeation sheet method established by Mchugh (Mchugh et al 1997) is to approximate the viscous fluid passing through the gap region as an attenuated non-viscous fluid passing through a row of holes, treating the hole as a curved surface element of the closed gap, and assuming that the surface element has a normal velocity, that is, the fluid can pass through the gap face. According to the orifice flow equation, the flow through the gap surface panel can be expressed as a linear function of the pressure difference between the blade pressure surface and the suction surface at the tip. The equation is as follows:

$$Q=C_Q A\sqrt{\frac{2\Delta p}{\rho}} \tag{4}$$

Where, C_Q is the discharge coefficient, and $0\le C_Q\le 1$, when $C_Q=0$, Indicates that the surface element is impermeable, Mchugh is 0.84 according to the experimental study of the ducted paddle; A indicating the area of the gap cell. Combined with the Bernoulli equation, the average percolation velocity V_{gap} through the gap element is obtained from the flow equation (5).

$$V_{gap}=\frac{Q}{A}=C_Q\sqrt{\frac{2\Delta p}{\rho}}=C_Q\left|\overrightarrow{V_{in}}\right|\sqrt{\Delta C_p} \tag{5}$$

$$\Delta C_p=\frac{\Delta p}{0.5\rho\left|\overrightarrow{V_{in}}\right|^2} \tag{6}$$

Where $\overrightarrow{V_{in}}$ is the relative inflow velocity and ΔC_p is the dimensionless coefficient of the pressure jump ∇p.

To satisfy the basic equation of the panel method, the gap face element is used as the radial extension of the blade tip face element and is connected to the inner wall surface of the duct, as shown in Fig.2. According to the assumption that the gap panel is permeable, combined with the permeation velocity equation (5) and the motion boundary condition, the source intensity of the gap panel can be expressed as:

$$\frac{\partial\phi}{\partial n}=-\overrightarrow{V_{in}}\cdot\vec{n}+C_Q\left|\overrightarrow{V_{in}}\right|\sqrt{\Delta C_p}\left(\vec{n}\cdot\vec{n}_{camber}\right) \tag{7}$$

Where $\vec{n}$ is the bin normal vector and $\vec{n}_{camber}$ is the normal vector of the mid-surface bin at the same chord position. The pressure coefficient ΔC_p is obtained through an iterative process. When the initial solution is solved, the gap surface element adopts the impenetrable wall condition to obtain an approximate initial solution. When solving again, the gap surface element uses equation (7) to update the blade surface through iteration. The pressure value of the element and the tip pressure difference ΔC_p until the convergence condition is satisfied.

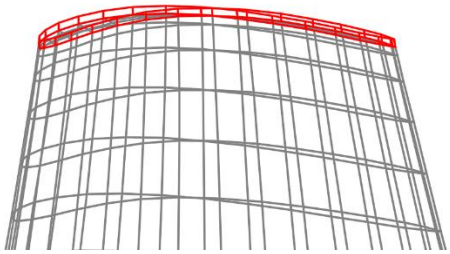

Fig.2 Geometric face of the gap (as a radial extension of the rotor tip unit)

3 Method validation

Due to the special application of the pump jet propulsor, there is a lack of published test data. Therefore, the more mature CFD simulation technology was used instead of the experimental method to verify the pump jet propulsor performance prediction method proposed in this paper and analyze the calculation results.

3.1 CFD method feasibility analysis

In order to verify the applicability of the CFD method for numerical simulation of a propeller with a stator, the front stator duct propeller with test data was used to verify the accuracy of the CFD method.

As shown in Fig.5, the geometric model contains 9 stator blades and 4 rotor blades, and the rotor diameter D is 0.254 m. The detail information of this calculation model can be obtained in the reference (Hughes M J et al.,1991).

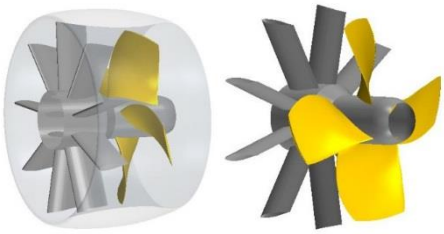

Fig.5 Geometric model of the duct propeller with pre-swirl stator blades

3.1.1 Grid partition of the computing domain

The computational flow field was divided into two cylindrical computational domains that simulated the infinity boundary and the inner domain that simulates the rotor's rotation. The diameter of outer domain is 15D selected to eliminate wall effect on the rotating area. The cylindrical surface was set as a symmetrical plane, and the speed inlet and the pressure outlet were both 10D away from the leading edge of the duct. The inner domain contained only the rotor, and the outer boundary was the inner wall of the duct. The upstream boundary took the duct entrance, and the downstream boundary was located between the stators and the rotors. The inner and outer domains delivered data through the interaction surfaces, as shown in Fig.6.

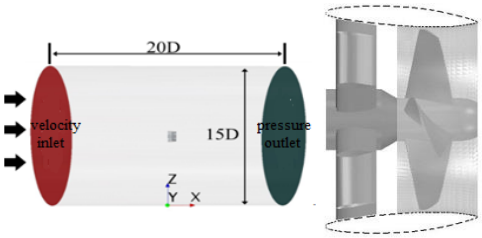

Fig.6 The whole computational domain and rotation domain

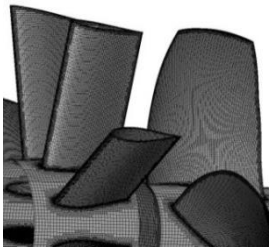

(a) stator and rotor

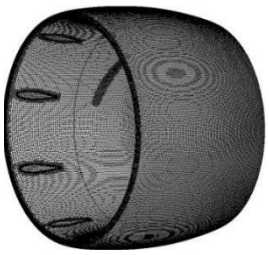

(b) duct

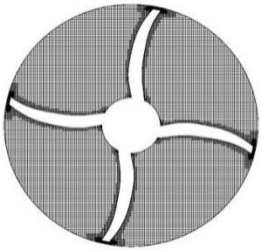

(c) cross section of rotor

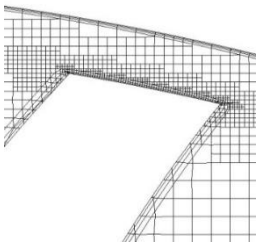

(d) rotor tip domain

Fig.7 The mesh generation

The computational domain and the near wall were discretized using Cartesian and prismatic grids respectively. Considering the influence of the boundary layer, the thickness of the first layer of the stator and rotor surface was set at 0.05 mm, with the corresponding Y+ value of 60 or so. In order to control the Y+ value and the number of grids, at least 3 layers of prismatic grids were arranged, and the ratio of thickness growth was 1.2 through inner layer to the outer layer. The edge line of each part, the top surface of the rotor, and the tip

* Corresponding author. E-mail address: 1557611797@qq.com (Kaiqiang Weng)

National Natural Science Foundation of China (51679052), National Defense Basic Research Project Funding Project (JCKY2016604B001).

clearance area were set densely, as shown in Fig.7. RNG k-ε turbulence model was selected to close the calculation equation, and the Multiple Reference Frame (MRF) model was used to forecast the steady performance. The diffusion phase used the central difference format, the convection phase used the first-order windward format, and the calculation method of flow field used the SIMPLEC algorithm.

3.1.2 Grid independence analysis

Following the work of Roy (Roy CJ et al 2013) on uncertainty research of Cartesian grid in viscous flow calculation, multiple sets of grids with various sizes have been established. The mesh size refinement rate r and the total number of grids satisfy the following relationship:

$$r = \left(\frac{N_{fine}}{N_{coarse}}\right)^{1/d},$$

Where N is the total number of grids and d is the space dimension of the problem. The mesh refinement rates in all three directions of each set of grids in the entire computing domain are consistent. In this paper, we set r with the value 1.2. Three different meshes were obtained with quantity of 2million,3.5million, and 6.11million, respectively. From the results shown in Table 1, as the number of grids increased, the errors of the thrust coefficient and torque coefficient between the calculated value and the test value are decreased. When the number of grids is more than 3.5 million, the calculation results have high accuracy, the error of *Kt-all* and *Kq* was less than 4%.

Table 1 The results of calculation and experiment

J=0.8	Test value	2 million	3.5 million	6.11 million
$K_{t\text{-}all}$	0.247	0.262	0.255	0.254
K_q	0.486	0.510	0.501	0.493
η	0.642	0.654	0.648	0.655

Fig.8 demonstrates the use of 6.11 million grids for forecasting the full condition hydrodynamic performance results. The calculated results of CFD are consistent with the experimental values within the design conditions, and deviations existed only if the advance speed coefficient is high. These results show that the CFD method has higher accuracy and reliability in the numerical simulation of the stator-like propeller, so it can be used to calculate the open water performance of pump jet propulsor and follow-up potential flow method validation.

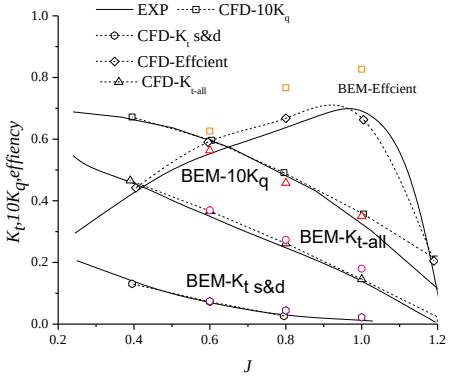

Fig.8 The comparison of open-water performance results on whole conditions

3.2 Discharge coefficient effect

Different discharge coefficients have different effects on the calculation results of the model. In this paper, different discharge coefficients are used to calculate the rotor ring volume, rotor and duct pressure distribution, and the discharge coefficient used in this paper is determined by comparative analysis.

The gap model relies on the dipoles and source points placed on the panel to interfere with adjacent panel, while the source point strength depends on the discharge coefficient C_Q, as shown in equation (7). Therefore, the magnitude of the discharge coefficient determines the degree of disturbance of the surrounding flow field by the gap flow model. In turn, c is taken as 0, 0.2, 0.4, 0.6, 0.84, and 1.0, and a gap flow model with different energy losses is established to analyze the influence of different pairs on adjacent surface panel. When C_Q=0, it means that the gap strip is impermeable to the wall; $C_Q = 1$ means that the fluid passing through the gap area has no energy loss, and $0 < C_Q < 1$ means that there is energy loss in the gap flow.

The calculation results of different gap models were taken under the condition of J=3.24, and the pressure distribution of the section of the rotor at $r/R = 0.98$ and the section of the duct at $\theta = 20°$ were intercepted, as shown in Fig.9. The results show that increasing the discharge coefficient increases the pressure value of the foliar as a whole, so that the pressure value of the leaf back near the leading edge increases, and the pressure value close to the edge decreases, so that the rotor has a pressure in the range of $0.2 < S/C < 1.0$,Jumping is more obvious. The overall pressure distribution on the surface of the duct is not sensitive to changes in C_Q. Only the interface between the inner surface of the duct and the gap model is affected. However, the pressure value changes to a lesser extent. Fig.10 shows the distribution of the circular volume with different C_Q gap models and without gap flow models. By comparison, it is found that the variation of the discharge coefficient has little effect on the prediction results of the overall performance of the rotor. However, compared with the results of the without gap flow model, the introduction of the gap flow model has a greater global impact on the rotor circular volume.

There is a significant increase in the value of the circular at each radial direction, indicating that the introduction of the gap model will increase the prediction results of rotor thrust and torque.

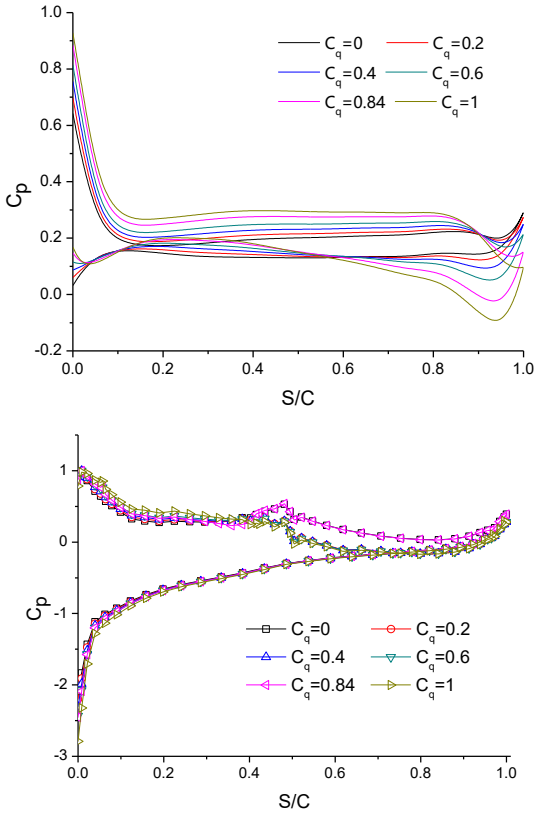

Fig.9 Pressure distribution of the rotor blade profile (r/R=0.98) under different discharge coefficients(top) Pressure distribution of the duct section ($\theta = 20°$) (below)

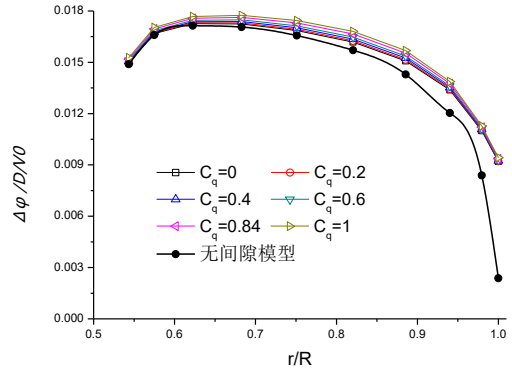

Fig.10 Radial circular distribution of the rotor under different discharge coefficients

The calculation results of the gap model (C_Q=0.84), the results of without gap flow model, and the CFD simulation results based on the viscous flow are compared. As can be seen from Figure 8, When C_Q=0.84, the calculated results agree well with the original model and the viscous flow calculation results, indicating that C_Q=0.84 can be used as the value chosen for the discharge coefficient.

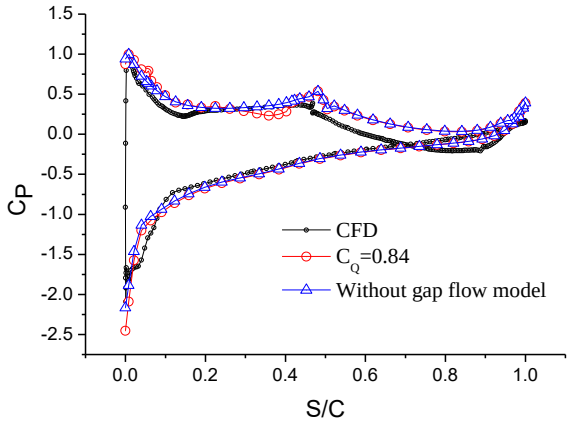

Fig.11 Duct section pressure distribution

Although the empirical coefficient value proposed by Kerwin is the gap flow model established by the lift surface method, However, from the pressure distribution of the rotor blade tip in Fig.9 and radial circular distribution of the rotor under different discharge coefficients in Fig.10 can be seen that C_Q=0.84 is also applicable to the gap flow model established by the panel method.

4 Calculation results and analysis of rear stator pump jet propulsor

The CFD method and the potential flow method were both used to predict the performance of Rear stator pump jet propulsor in this paper. A total of four working conditions were calculated, and the advanced speed coefficient J was 1.29, 1.94, 2.59, and 3.24, respectively. The influence of the gap flow model on the calculation results is analyzed. Based on the numerical model of the pump jet propulsor, the additional model is introduced respectively, and the calculation results of pressure distribution, circular distribution and performance index are compared with the results of CFD simulation based on viscous flow.

4.1 Rear stator model

The model contains 11 rotor blades and 9 stator blades, rotor maximum diameter D_r is 0.238 m, spinning speed n is 2000 rpm, and the minimum clearance between the rotor tip and the duct is 3 mm. The total number of grids calculated by the CFD method is 9.44 million and the number of rotating domain grids is 4.17 million. The surface mesh is shown in Fig.12 and the mesh of the potential flow method is shown in Fig.13. The number of grids for both rotor and stator blade is 32×10, and the number of grids for hub and duct is 56×33 and 60×99, respectively.

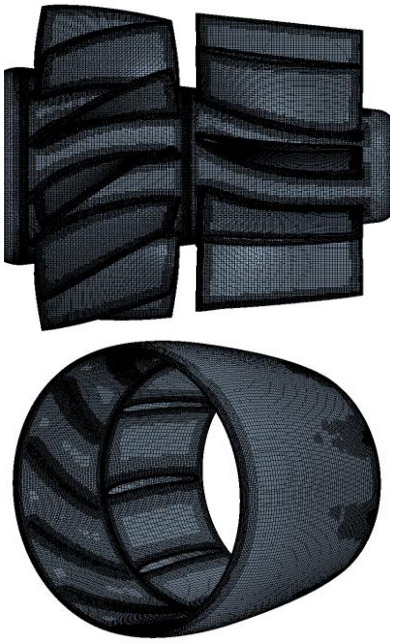

Fig.12 The grid of CFD calculation model

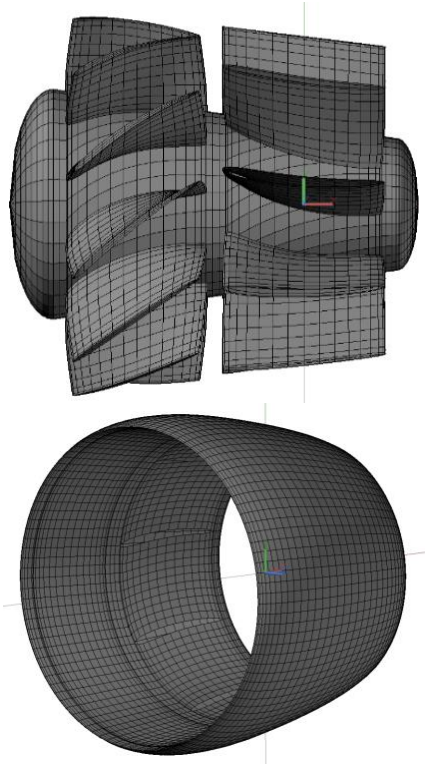

Fig.13 The mesh distribution of potential flow calculation model

4.2 Pressure and circular distribution

In this paper, two working conditions of J=1.94 and J=3.24 are selected, and two cases of the presence or absence of the gap flow model are calculated respectively. The pressure distribution of the rotor at r/R=0.88 and r/R=0.98 was analyzed to further compare the main influence range of the gap flow model. At the same time, the potential flow calculation results are compared with the CFD calculation results. As shown in Fig.14 and 15, S/C represents the dimensionless chordwise distance of the center point of the surface panel from the rotor leading edge.

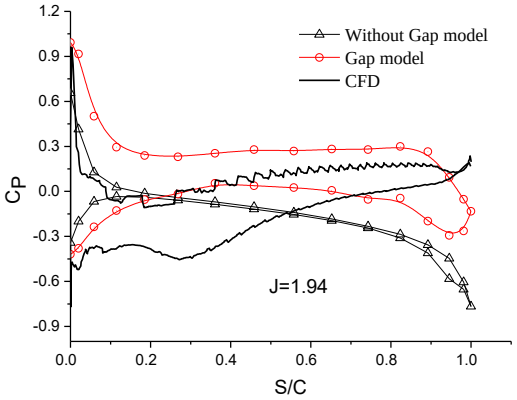

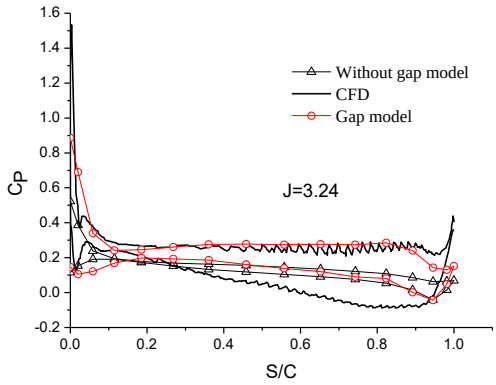

(a)r/R=0.98

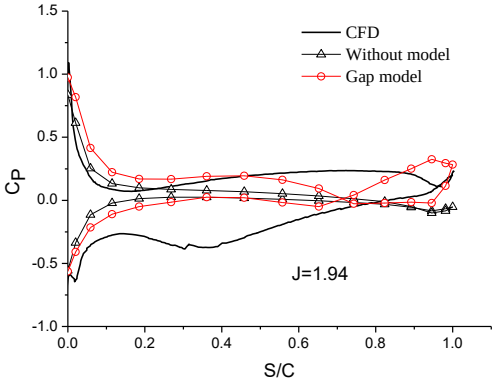

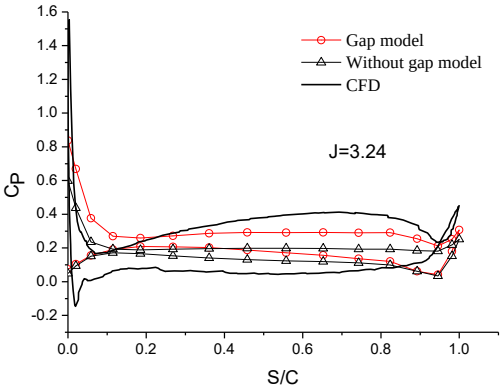

(b)r/R=0.88

Fig.14 Pressure distribution of the rotor blade at (a) r/R=0.98 and (b) r/R=0.98

As can be seen from the rotor pressure distribution, the gap flow model has a significant effect on rotor blade pressure distribution. As the radius of the leaf profile increases, the gap flow model has a greater impact on the

profile load near the rotor tip. It can be seen from the Fig.14 that the calculation result considering the influence of the gap flow significantly increases the pressure difference between the leaf back and the leaf surface, so that the variation trend of the section pressure along the chord direction is closer to the calculation result of the viscous flow. This is because during the actual fluid flow, due to the gap between the rotor tip and the inner wall surface of the duct, the fluid is affected by the boundary layer of the duct and the top surface of the rotor. The flow velocity of the rotor blade tip on the suction side and the pressure side is quite different. The gap flow model considers the influence of the gap flow by introducing the discharge coefficient, which is more in line with the flow of the real fluid. At the same time, by comparing the calculation results under different advanced speed conditions, the influence of the gap model is more significant at low advanced speed. In summary, the introduction of the gap model greatly improves the pressure distribution of the rotor section, and compensates for the fact that the pressure difference of the leaf profile is small when using the potential flow; At the same time, it can be seen that the gap model has a greater influence on the rotor near the blade tip, and has less influence on the pressure distribution of the rotor profile near the blade root.

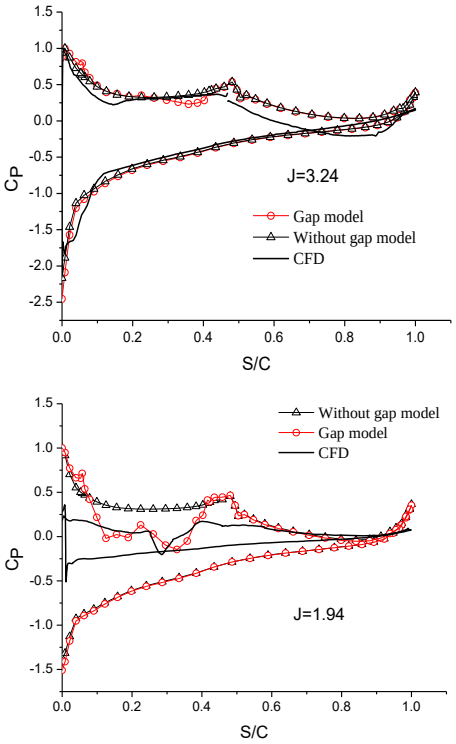

Fig.15 Pressure distribution in longitudinal section of duct ($\theta = 20°$)

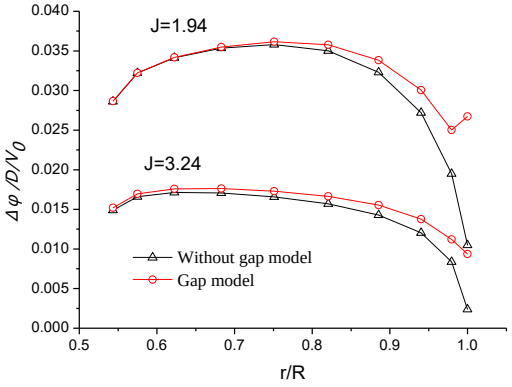

Fig.16 Rotor radial circular distribution

The above figure calculates the pressure distribution on the surface of the duct under different advanced speed coefficients. It can be seen from the pressure distribution in the Fig.15 that the gap flow model has little effect on the pressure distribution on the outer surface of the duct, and the model only affects the inner surface of the duct above the rotor. When the incoming flow velocity is high, the Reynolds number is larger and the boundary layer thickness is smaller. The potential flow calculation result is basically consistent with the CFD calculation result; When the incoming flow velocity is small, the gap flow model is introduced at the top end of the rotor, and the influence of fluid viscosity is considered. At this time, the potential flow calculation results in the axial region of the rotor, and the pressure value of the inner wall surface of the duct decreases, and the trend of CFD calculation results be consistent.

It can be seen from the chord-to-loop distribution of the rotor that the introduction of the gap flow model makes the circular distribution at the rotor tip no longer tend to zero, which is consistent with the actual situation of the flat-top blade, and the increase of the circular value makes the rotor the thrust and torque will also increase.

4.3 Open water performance prediction results

This study considered five conditions, in which the advance speed coefficients were 1.29, 1.94, 2.59 and 3.24. The pump jet propulsor stator, rotor, and overall performance calculations were compared with the CFD calculations shown in Fig.17 and Fig.18.

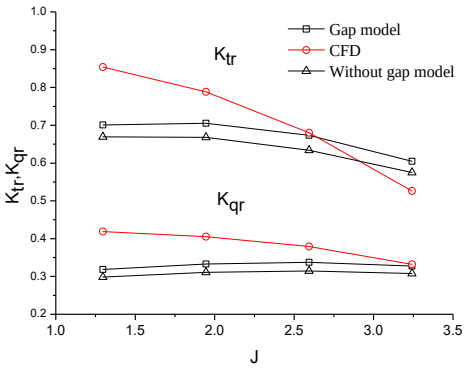

(a) Rotor

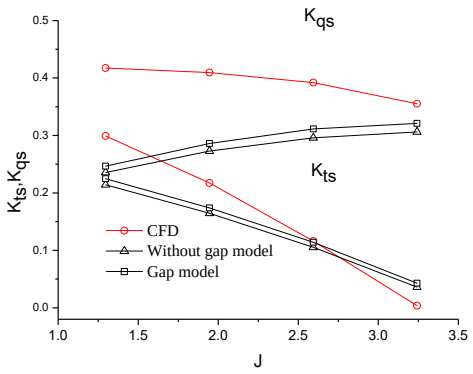

(b)Stator

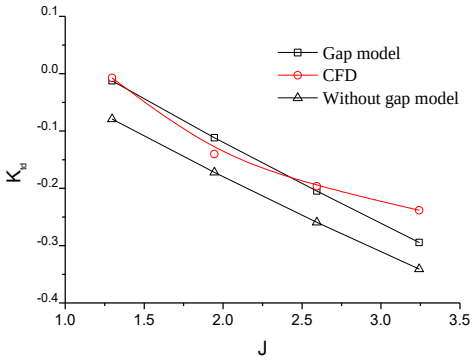

(c) Duct

Fig.17 Performance prediction results of rotor, stator and duct.

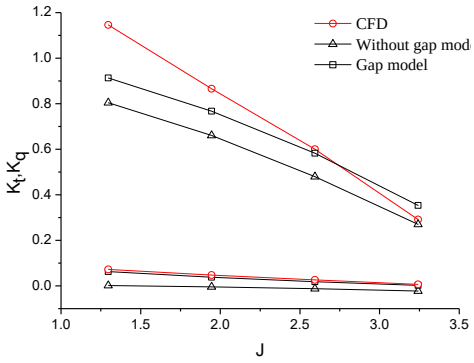

Fig.18 Thrust coefficient and torque

As we can see from the Fig. 17 and Fig. 18, the thrust and torque coefficients of the no gap flow model were quite different from the CFD results, especially when the flow rate was smaller, the difference is more obvious. The introduction of the gap flow model increases the thrust and torque of the rotor, stator and duct. Especially at low advanced speeds, the calculation of the thrust coefficient of the duct is closer to the calculation of the viscous flow. For the open water performance of the pump jet propulsor, the introduction of the gap model makes the calculation result closer to the calculated value of the viscous flow. It shows that the introduction of the gap model plays an important role in the calculation of the pump jet propulsor. However, at low advanced speeds, there is still a difference between the calculated value of the influence of the gap flow and the calculation result of the CFD. This is because the gap flow model mainly affects the rotor tip load. The overall hydrodynamic performance of the pump jet propulsor has only been improved.

5 Conclusions

Based on the potential flow theory, this paper presents a method of predicting the steady hydrodynamic performance of a pump jet propulsor based on the panel method. For the first time, a gap flow model suitable for flat-topped blades is given. The rotor tip was processed in different ways, and the calculation results of the pressure distribution, circular distribution, and the performance indexes were analyzed. The following conclusions were obtained.

1) Comparing the calculation results of the panel method with the CFD results, the theoretical calculation results are in good agreement with the viscous flow results, and the effectiveness of the pump-jet interference model proposed in this paper is verified.

2) The introduction of the gap flow model makes the pressure distribution at the tip of the rotor closer to the viscous flow result, which is more realistic with the overall circular distribution of the blade, and the smaller the velocity coefficient, the more obvious the influence.

3) Although the lack of experimental data cannot accurately quantify the accuracy of the prediction method, from the comparison of performance indicators, this method can obtain the prediction conclusions that are basically consistent with the CFD method, and the occupied resources are much smaller than the CFD method.

REFERENCES

Baltazar J, Falcao de Campos J A C andBosschers J. Potential flow modelling of ducted propellers with a panel method[C]. Fourth International Symposium on Marine Propulsors, Texas, USA, 2015.

Gerard P. Mchugh. Advances in Ducted propulsor Analysis Using Vortex-Lattice Lifting-Surface Techniques. Naval Engineer Thesis, Massachusetts Institute of Technology, Department of Ocean Engineering, 1997.

Hughes M J,Kinnas S A. An analysis method for a ducted propeller with pre-swirl stator blades[C]// Proceedings of Propellers & Shafting'91 Symposium. Virginia Beach: SNAME, 1991:15-1~15-8.

Kawakita, C., Hoshino, T., Hydrodynamic Analysis of Ducted Propeller with Stator InSteady Flow Using a Surface Panel Method, Transactions of the West-Japan Society of Naval Architects, No. 96, 1998.

Roy C, Heintzelman C, Roberts S. Estimation of Numerical Error for 3D Inviscid Flows on Cartesian Grids[J]. 2013.